國立嘉義大學生命科學院 105 年度
學生學術研究成果優良海報評選獲獎名單

時間：105 年 6 月 1 日

大學部

食品科學系					
第二名	吳峻瑋、謝鈞任	第三名	施凱瀞、張嘉瑄		
生物資源學系					
第一名	李孟榛	第二名	廖凱鋐	第三名	張家豪
微生物免疫與生物藥學系					
第一名	張立展	第二名	王仁軒	第三名	王翔昱

碩士班

食品科學系					
第一名	Nguyen Xuan Hoang	第二名	林姿廷	第三名	鄭冠威
水生生物科學系					
第一名	徐正翰	第二名	蘇意婷	第三名	劉偌凡
生物資源學系					
第一名	張凱筌	第二名	涂翔議	第三名	黃毓淨
生化科技學系					
第一名	吳玉萍	第二名	王泰景	第三名	蔡泓岳
微生物免疫與生物藥學系					
第一名	王守琮	第二名	林鴻志	第三名	張家源

微生物免疫與生物藥

學系學士班

Synthesis of novel norcantharimide derivatives and evaluated for their anti-cancer activity

Li-Chan Chang (張立展), Meng-Chin Chen (陳孟勤) and Jin-Yi Wu (吳進益)*

Department of Microbiology, Immunology and Biopharmaceuticals, National Chiayi University, Chiayi, Taiwan

INTRODUCTION

Hepatocellular carcinoma (HCC) is one of the most common malignancies and results in high mortality; an estimated 748,300 new cases and 695,900 deaths occur worldwide in a single year as a result. Only a very small subset of HCC patients can be cured with surgery, while majority of patients with advanced HCC rely on chemotherapy and radiology. Norcantharidin (NCTD) is the demethylated analogue of cantharidin (CTD), it possesses less cytotoxicity and it has been used as anticancer drug to inhibit cell proliferation, induce apoptosis for several kinds of cancer, such as liver cancer, colorectal cancer, bladder cancer, breast cancer and ovarian cancer. However, its poor solubility and absorption in the human body let it has a short biological half-time and may be eliminated rapidly after oral or intravenous administration. In order to overcome this shortcoming, we synthesized a series of new norcantharimide derivatives, to evaluate their anticancer activity on human cancer cell lines.

MATERIALS AND METHODS

Chemistry

Scheme I: Synthesis of NCTD and its derivatives.

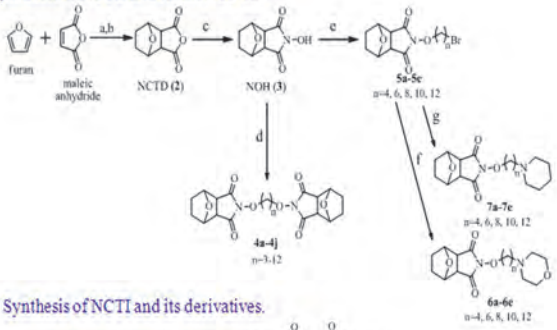

Scheme II: Synthesis of NCTI and its derivatives.

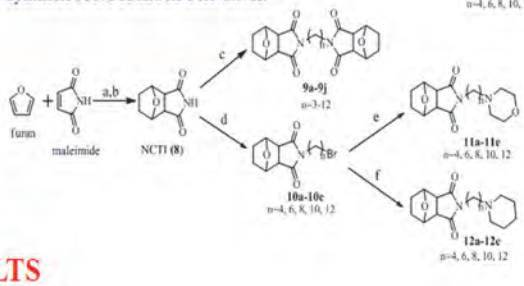

RESULTS

Table 1. Cell viability of NCTD and its derivatives in four cancer cell lines for 48 h.

Compound	n	IC_{50} (μM)			
		HepG2 (liver)	SW480 (colon)	HT29 (colon)	BFTC905 (bladder)
NCTD	-	45.3 ± 1.7	59.9 ± 2.2	16.0 ± 1.0	22.5 ± 1.3
4a	3	>50	>50	>50	>50
4b	4	>50	>50	>50	>50
4c	5	15.6 ± 0.9	28.6 ± 0.6	17.7 ± 0.4	22.0 ± 0.6
4d	6	21.8 ± 1.1	20.8 ± 0.9	23.0 ± 0.5	20.9 ± 0.8
4e	7	20.3 ± 0.8	36.9 ± 1.7	19.0 ± 0.5	20.0 ± 0.6
4f	8	10.9 ± 1.2	23.9 ± 0.9	17.1 ± 2.0	17.3 ± 1.3
4g	9	11.7 ± 0.3	26.1 ± 1.0	14.7 ± 0.8	18.4 ± 0.8
4h	10	9.6 ± 0.4	21.4 ± 0.5	6.4 ± 1.1	9.8 ± 0.1
4i	11	9.5 ± 0.2	22.1 ± 0.9	5.5 ± 0.1	9.5 ± 0.3
4j	12	8.2 ± 1.2	15.9 ± 5.9	4.9 ± 1.1	5.0 ± 0.2
6a	4	47.4 ± 2.4	>50	22.8 ± 1.5	28.7 ± 1.3
6b	6	19.5 ± 1.7	32.6 ± 2.9	19.7 ± 1.6	21.7 ± 1.3
6c	8	25.3 ± 1.8	33.9 ± 2.4	19.4 ± 2.5	20.8 ± 1.6
6d	10	18.7 ± 2.5	26.6 ± 1.5	20.8 ± 0.6	18.6 ± 1.8
6e	12	7.9 ± 0.2	15.6 ± 0.3	12.2 ± 1.0	7.0 ± 0.4
7a	4	>50	>50	>50	>50
7b	6	20.2 ± 1.7	44.9 ± 0.7	17.0 ± 1.3	18.4 ± 1.1
7c	8	>50	>50	>50	20.2 ± 1.0
7d	10	35.2 ± 1.6	>50	>50	22.6 ± 1.0
7e	12	2.2 ± 0.2	8.0 ± 0.1	3.9 ± 0.6	5.7 ± 0.2
9a	3	>50	>50	>50	>50
9b	4	>50	>50	>50	>50
9c	5	>50	>50	>50	>50
9d	6	>50	>50	>50	>50
9e	7	>50	>50	>50	>50
9f	8	>50	>50	>50	>50
9g	9	10.8 ± 0.9	>50	>50	>50
9h	10	11.1 ± 0.4	>50	>50	>50
9i	11	9.5 ± 0.8	>50	>50	>50
9j	12	7.3 ± 1.2	>50	7.2 ± 2.4	>50
11a	4	>50	>50	>50	>50
11b	6	>50	>50	>50	>50
11c	8	>50	>50	>50	>50
11d	10	44.4 ± 0.5	>50	>50	>50
11e	12	19.4 ± 0.6	25.6 ± 2.9	18.8 ± 2.0	18.0 ± 2.0
12a	4	>50	>50	>50	>50
12b	6	>50	>50	>50	>50
12c	8	>50	>50	>50	>50
12d	10	41.2 ± 0.4	39.3 ± 1.8	38.4 ± 1.7	35.4 ± 1.7
12e	12	11.3 ± 1.7	14.9 ± 1.8	13.6 ± 1.1	14.2 ± 1.2

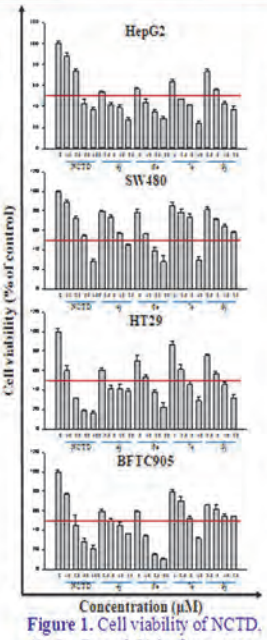

Figure 1. Cell viability of NCTD, **4j**, **6e**, **7e** and **9j** in four cancer cell lines for 48 h.

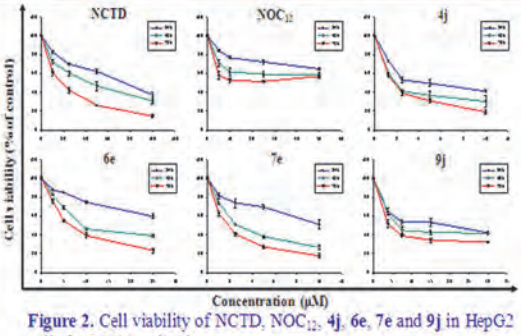

Figure 2. Cell viability of NCTD, NOC_{12}, **4j**, **6e**, **7e** and **9j** in HepG2 cells for 24, 48 and 72 h.

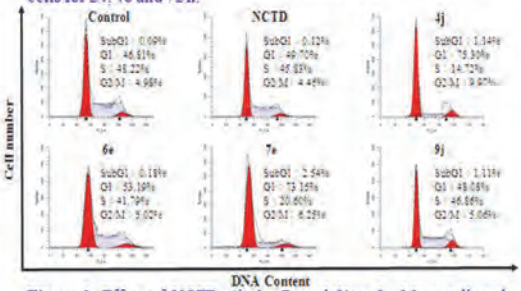

Figure 3. Effect of NCTD, **4j**, **6e**, **7e** and **9j** at 5 μM on cell cycle distribution in HepG2 cells for 48 h.

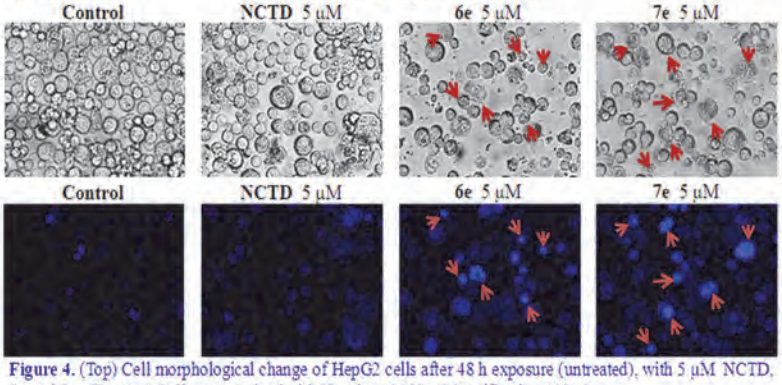

Figure 4. (Top) Cell morphological change of HepG2 cells after 48 h exposure (untreated), with 5 μM NCTD, **6e** and **7e**. (Bottom) Cells were stained with Hoechst 33258. (Magnification 400 ×)

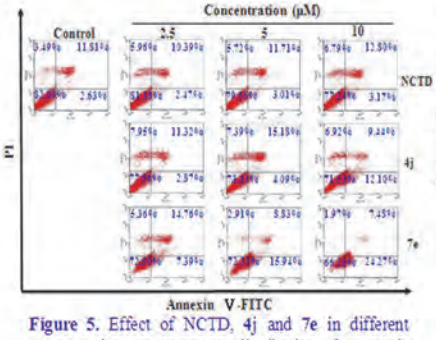

Figure 5. Effect of NCTD, **4j** and **7e** in different concentration on percentage distribution of apoptotic cells in HepG2 cells for 48 h.

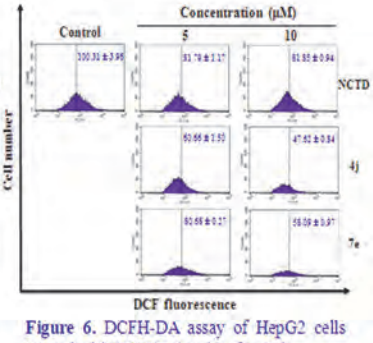

Figure 6. DCFH-DA assay of HepG2 cells treated with NCTD, **4j** and **7e** for 48 h.

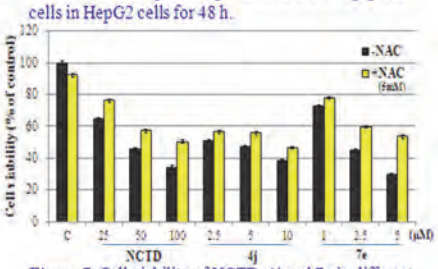

Figure 7. Cell viability of NCTD, **4j** and **7e** in different concentration in HepG2 cells after pretreated with NAC (5mM) for 48 h.

Table 2. Cell viability of NCTD, **4j** and **7e** in HepG2 cells after pretreated with NAC (5mM) for 48 h.

Compound	Tumor cell lines IC_{50} (μM)		
	Without NAC	With NAC (5mM)	SI*
NCTD	45.3 ± 1.7	101.4 ± 4.2	2.24
4j	3.3 ± 0.2	8.1 ± 0.6	2.47
7e	2.2 ± 0.2	6.9 ± 1.0	3.09

*SI = With NAC IC_{50}/ Without NAC IC_{50}

CONCLUSIONS

In this study, we synthesized forty new norcantharimide derivatives **4a-j**, **6a-e**, **7a-e**, **9a-j**, **11a-e**, and **12a-e**. We found that these compounds which are more hydrophobic have much stronger anticancer activities than NCTD. Thus, we revealed that **4j** and **7e** could be potential candidate for new anticancer drug on hepatocellular carcinoma.

Luteolin affects the physiological characteristics of dendritic cells

Ren-Xuan Wang, Jing-Jing Chuang
Department of Microbiology, Immunology and Biopharmaceuticals, National Chiayi University

Introduction

Dendritic cells (DCs) are the major antigen-presenting cells. They are regulators of both innate and acquired bridges of immune system. Luteolin, a kind of flavonoid, exists in many types of plants including fruit, vegetable, and medicinal herb. It has activity of estrogen, pro-oxidant, anti-oxidant, and anti-inflammation. In this study, we investigated the effect of luteolin on mature DC2.4 (mDC2.4).

Materials and Methods

Cell culture
DC2.4 cells were cultured in RPMI1640 containing 20 % of heat-inactivated fetal bovine serum.
Luteolin
Mitomycin C (MMC)
Cell viability was assessed by MTT and MTS assays
Treated cells were incubated with MTT solution for 2 hrs, and then the MTT formazan in DMSO was measured the absorbance at 570 nm.
T-cells were co-culture with DCs for 5 days, and T-cell proliferation was assessed by MTS assay.
Cell cycle was detected by BrdU and PI assays
Surface molecules were analyzed by flow cytometer
The major histocompatibility complex (MHC) and costimulatory molecules on DCs were analyzed by flow cytometer.

Results

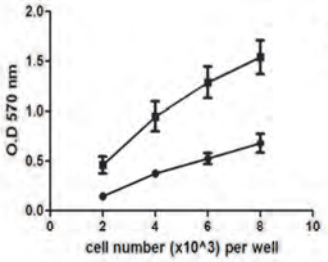

Figure 1. The cell-growth curve of DC2.4 was dependent on cell number. Cells were seeded with different cell number and cultured for 24 and 48 hrs. Cell proliferation were assessed by MTT assay.

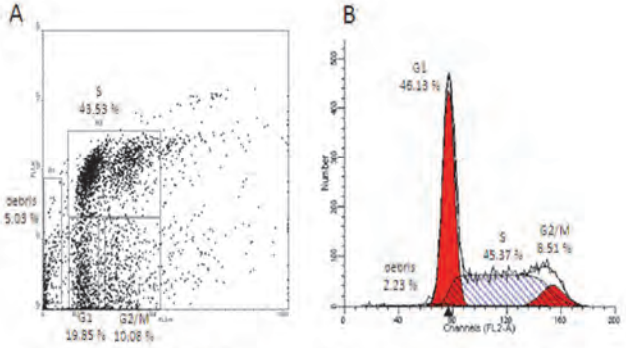

Figure 2. The 45% of DC2.4 was in the S phase. (A) The cell cycle was detected by BrdU assay. (B) The cell cycle was detected by PI assay.

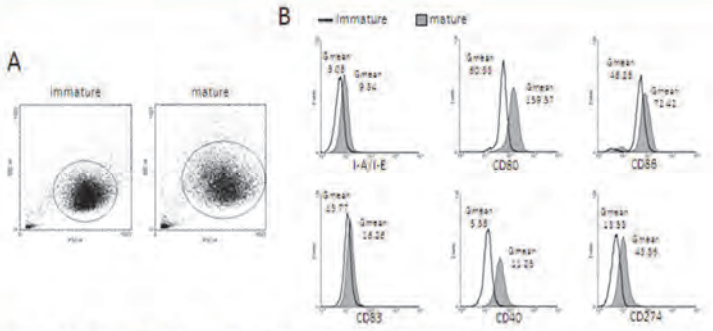

Figure 3. The mDC2.4 could significantly express MHC and costimulatory molecules. The maturation of DC2.4 was induced by lipopolysaccharides (LPSs) and tumor necrosis factor alpha (TNF-α). (A) The cell size, granularity and (B) expressions of surface molecules (I-A/I-E, CD80, CD86, CD83, CD40 and CD274) were analyzed by flow cytometer.

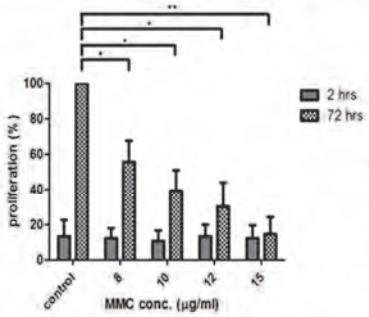

Figure 4. MMC potentially inhibited the proliferation of mDC2.4. The mDC2.4 was treated with different concentration of MMC for 1 hr, and then cultured for 2 and 72 hrs. Cell viability was assessed by MTT assay. Statistical analysis was performed by paired t-test. *, $p < 0.05$; **, $p < 0.01$. N=3

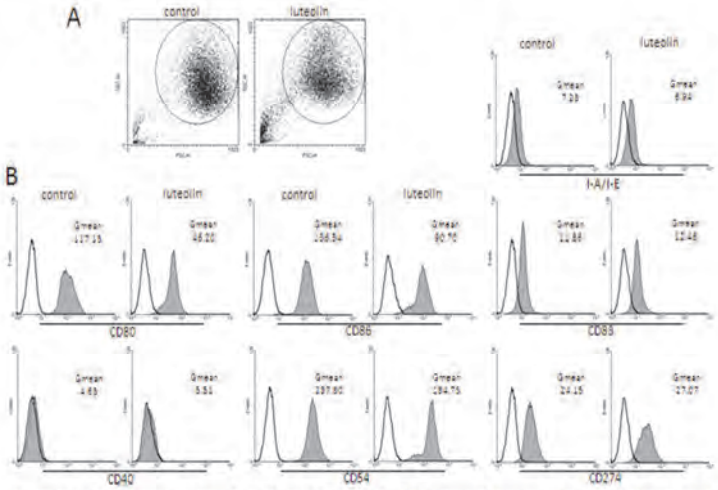

Figure 5. The expression of I-A/I-E, CD86 and CD80 was decreased on luteolin-treated mDC2.4. The mDC2.4 was treated with 40 μM luteolin for 18 hrs. The expressions of surface molecules (I-A/I-E, CD80, CD86, CD83, CD40, CD54 and CD274) was analyzed by flow cytometer. The expressions of surface molecules were shown by filled histograms. Isotype control was shown by a solid line.

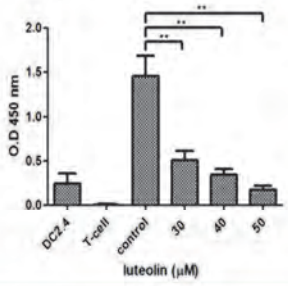

Figure 6. Luteolin-treated mDC2.4 strongly inhibited T-cells proliferation. After treatment of mDC2.4 with luteolin, and then cells were post-treated with 12 μg/ml MMC for 1 hr. The mDC2.4 co-cultured with T-cells for 5 days. Cell proliferation was assessed by MTS assay. Statistical analysis was performed by paired t-test. **, $p < 0.01$.

Conclusion

These results suggest that the downregulation of I-A/I-E, CD86 and CD80 on luteolin-treated mDC2.4 is a potential mechanism of the effect for inhibition of T-cell response.

Trichostatin A引發人類膀胱癌細胞死亡機制探討與小鼠原位膀胱癌之治療效果評估

Xiang-Yu Wang (王翔昱) and Yi-Wen Liu, Ph.D. (劉怡文 博士)

Department of Microbiology, Immunology and Biopharmaceuticals, Collage of Life Sciences, National Chiayi University

Introduction

膀胱癌為世界常見癌症之一，雖然不是致死率前3名的癌症，但其治療後復發率非常高。現今主要治療膀胱癌的方式包括經尿道刮除、膀胱灌注藥物、放射線治療及利用多種藥物系統性治療，希望降低癌細胞轉移的可能，因此利用藥物減緩膀胱癌的惡化或是轉移，是現今對於膀胱癌研究的重要方向。過去的文獻指出histone deacetylases (HDACs)的過度表現常常被發現在人類癌症細胞中，而HDAC抑制劑(HDACi)可以作用在癌細胞以誘導細胞生長停滯和細胞凋亡，Trichostatin A (TSA) 即為HDACi的一種藥物，有不少研究指出TSA可誘導卵巢癌、大腸癌以及肺癌細胞死亡。

Aim

探討Trichostatin A (TSA)造成人類膀胱癌細胞死亡的機制，並利用動物實驗探討TSA對於小鼠原位膀胱癌之治療效果評估。

Materials and Methods

Cell Culture

- Cell viability assay (MTT assay)
- **Trichostatin A影響5637細胞相關路徑探討**
- Detect mitochondrial membrane potential change by Flow cytometry
- Western Blotting
- RT-PCR

Animal experiment

Results

Trichostatin A對人類膀胱癌細胞生長與型態的影響

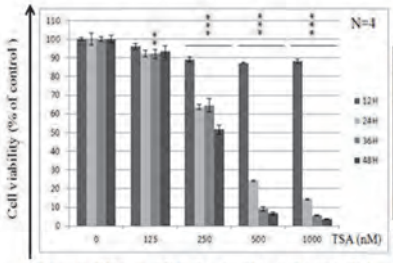

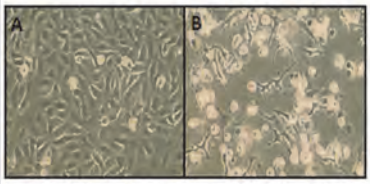

Figure 1. TSA對人類膀胱癌細胞5637細胞株的細胞毒性。

Figure 2. 5637細胞處理TSA後型態的變化，細胞處理時間為24小時(Magnification 200X)。(A) Control (B) 500 nM TSA。

經由細胞存活率試驗測試，在TSA處理人類膀胱癌5637細胞株12小時即有存活率下降的狀況，但24與48小時後，細胞的存活率明顯下降。而其作用24小時後的IC50大約介於250 nM與500 nM之間 (Figure 1)。而細胞在處理500 nM TSA 24小時後，與控制組相比，細胞出現許多類似樹突之觸角，形狀也變得狹長較不規則 (Figure 2B)，而且目視下可明顯觀察到細胞存活數量降低，因此證實TSA能使細胞的存活率下降。

Trichostatin A造成p21蛋白在藥物處理12小時表現量上升

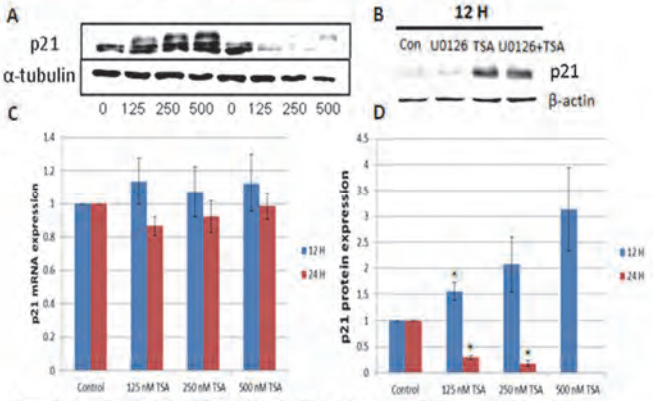

Figure 3. (A) 經TSA分別處理5637細胞12小時與24小時後，細胞內p21蛋白表現隨濃度及時間上升。(B) 經TSA與U0126分別處理5637細胞12小時後，細胞內p21蛋白表現量 (TSA 500 nM, U0126 10 μM)。不同濃度的TSA處理下，5637細胞株內 (C)mRNA與 (D) 蛋白質表現量。(*=p<0.05, **=p<0.01,與control相比)

- 細胞內p21蛋白表現量隨濃度及時間上升 (Figure 3A)。
- 使用ERK1/2 inhibitor U0126處理後相較於單處理TSA的組別，p21蛋白表現量並無明顯降低 (Figure 3B)。因此推論，TSA並未經由ERK1/2影響p21的表現量。
- p21 mRNA表現量在統計上並無明顯差異，因此判斷處理TSA後並無顯著改變p21 mRNA 表現量 (Figure 3C)。
- p21蛋白表現於量12小時的藥物處理時間有增加的趨勢，而到了24小時則呈現顯著下降的情形 (Figure 3D)。因此推論，TSA確實能造成p21蛋白在12小時的表現量上升，但並非p21 基因轉錄活性增加之故。

Trichostatin A處理人類膀胱癌細胞5637後細胞粒線體膜電位變化

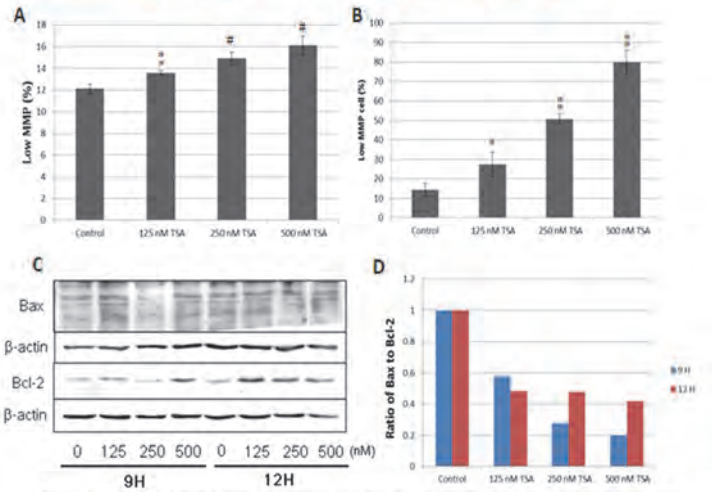

Figure 4. Trichostatin A處理人類膀胱癌細胞5637細胞株造成粒線體膜電位下降比例上升 (A) 12 H (B) 24H。(C) 在不同濃度及時間TSA處理下，Bax與Bcl-2的蛋白表現量。(D) Bcl-2與Bax蛋白表現量比值。(*p<0.05, **p<0.01, ≠p<0.001, 與control相比)

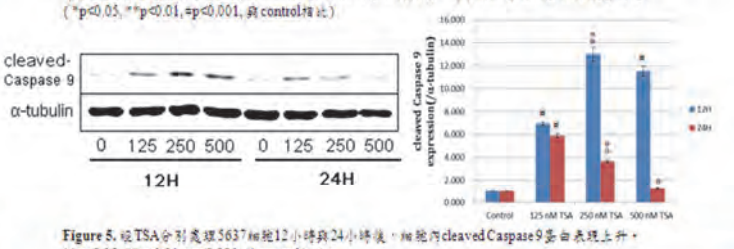

Figure 5. 經TSA分別處理5637細胞12小時與24小時後，細胞內cleaved Caspase9蛋白表現上升。(*p<0.05, **p<0.01, ≠p<0.001, 與control相比)

- TSA處理人類膀胱癌5637細胞12小時後，細胞粒線體膜電位下降的細胞群比例即有些微上升，而在TSA處理24小時後，膜電位下降的細胞群比例有非常明顯增加 (Figure 4A, 4B)，再加上cleaved Caspase9表現量的上升 (Figure 5)，因此推論TSA處理人類膀胱癌細胞5637細胞株走向細胞凋亡可能經由粒線體之內途徑間接導致。
- 文獻指出Bax與Bcl-2的高比值主要能驅動粒線體細胞膜電位的下降與細胞凋亡的現象，而本次實驗Bax與Bcl-2的蛋白表現量比值 (Bax/Bcl-2) 呈現下降的情形 (Figure 4C, 4D)，因此推論TSA處理5637細胞後，導致粒線體膜電位下降應與Bax與Bcl-2較無關聯。

小鼠原位膀胱癌實驗模式

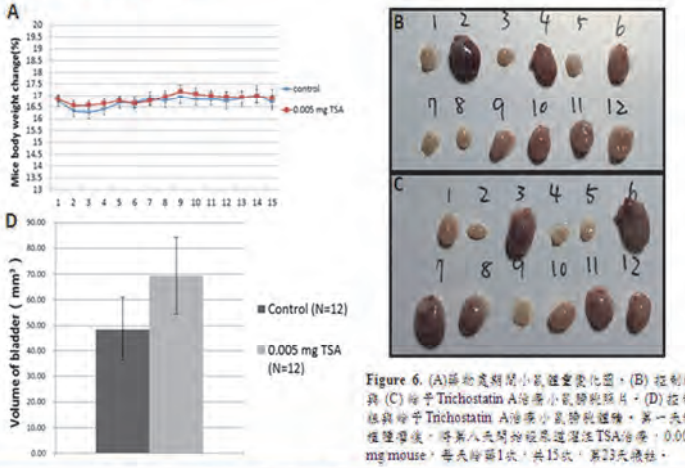

Figure 6. (A)藥物處理期間小鼠體重變化圖，(B) 控制組與 (C) 給予Trichostatin A治療小鼠膀胱腫瘤。(D) 控制組與給予Trichostatin A治療小鼠膀胱腫瘤。第一次腫瘤植入後，將第八天開始經尿道灌注TSA治療，0.005 mg/mouse，每天給藥1次，共15次，第23天犧牲。

- 治療期間小鼠體重並無明顯變化，犧牲後TSA處理組別小鼠膀胱平均體積較控制組組別大 (Figure 6)。以此結果推論，TSA在活體小鼠膀胱原位癌模式當中並沒有明顯的療效。

Conclusion

TSA處理人類膀胱癌5637細胞株後，會使p21蛋白表現量上調，因此可能會影響細胞週期之進行，而死亡機轉會藉由粒線體膜電位的降低導致細胞凋亡。但在小鼠的活體膀胱原位癌實驗中，施以經尿道膀胱灌注給藥，並未觀察出具有治療膀胱腫瘤的效果。

微生物免疫與生物藥學系碩士班

Evaluation of Urinary Bladder Fibrogenesis in Mouse Model of Long-term Ketamine Injection

Shou-Tsung Wang (王守琮) and Yi-Wen Liu (劉怡文)

Department of Microbiology, Immunology and Biopharmaceuticals (DMIB), National Chiayi University

Abstract

Long-term ketamine abuse has been shown to affect the lower urinary tract and result in interstitial cystitis-like syndrome. However, the causative mechanism of ketamine-induced dysfunction is still not clear. This present study was to investigate the physiological, histological and molecular changes on ketamine-induced cystitis (KIC) in a mouse model. Both male and female Balb/c mice were separately distributed into the control (normal saline) and ketamine groups which received ketamine hydrochloride (100 mg/kg/day) daily by intraperitoneal injection for a total period of 20 weeks. In each group, the urine was analyzed by GC-MS to measure the concentration of ketamine and its metabolites. Urinary frequency and urine volume were examined to investigate the urinary voiding functions. Mice bladders were excised for cDNA microarray and histological stains. The ketamine and metabolites were detected only in ketamine-treated mice urine. The voiding interval was decreased at the male mice group after 20-week ketamine administration. Moreover, the result of cDNA array analysis revealed a number of gene expressions involved in chronic wound healing response and collagen accumulation, which were closely related to fibrosis progression in the connective tissue. In HE stain of bladder tissue, the ketamine-injected mice showed prominently denser blood vessel distribution in the submucosal layer. However, the results of Masson's trichrome and Periodic acid–Schiff (PAS) stain showed no significant difference on protein expression of collagens as well as mucosubstances, suggesting the pathology may still stay in the initial stage. Taken together, based on the evidence in our experiment, we may build up a mechanism that delineates fibrosis formation of urinary bladder induced by the pathogenesis of ketamine abuse.

Introduction

Ketamine

- Ketamine is a common abuse drug for rave party. It is easy to obtain illegally and is very hallucinogenic (dream-like states or deep trance called as "K-hole"). At present, ketamine was prohibited and listed as the third-grade controlled drug since 1999 in USA, and 2002 in Taiwan.

Addiction 2012; 107:27-38

Ketamine-induced cystitis (KIC)

- Cases of bladder dysfunction among recreational ketamine users were first reported around 2007 from two literatures that related to ketamine-associated cystitis (KIC). Since then, many articles have indicated that ketamine affects the urinary system in clinical cases, involving increased urination frequency, nocturia, urgency, suprapubic discomfort during micturition and hematuria.

BJU Int. (2008);102:1616–1622 LUJ (2009);16:325-329

cDNA microarray analysis

- Mouse OneArray® v2.1 (Phalanx Biotech Group, Taiwan) with 26,423 genome probes was used to analyze the differentially expressed genes (DEGs) between ketamine-treated group and control group. The criteria with $\log_2$|fold change| ≥ 0.5 and *p*-value < 0.05 were adopted for further analysis.

Aim

- To evaluate the effects of long-term ketamine treatment on KIC mouse model according to the results of urinary bladder physiology, tissue morphology and gene expression, as well as try to find out the plausible bio-markers of KIC.

Materials and Methods

BALB/c mice (6 weeks old)
both male and female

↓

Ketamine → 100 mg/kg/day, intraperitoneal injection
Control → injection of normal saline

↓

After 20 weeks, mice were euthanized

Physiological exam	Tissue pathology	cDNA microarray
Body weight Voiding behavior Urine Ketamine concentration	H&E Masson's trichrome	DEG Biomarkers

Results

Concentration examination of ketamine and its metabolites in mouse urine

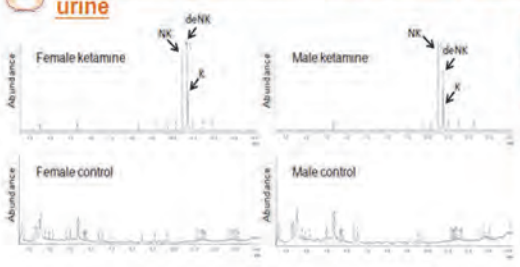

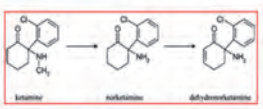

Shimadzu GCMS-QP2010 system

Group	K (ppm)	NK (ppm)	deNK (ppm)
Female	108 ± 9.9	336 ± 17.1	1332 ± 66.0
Male	173 ± 9.1	599 ± 8.4	1286 ± 13.7

GC-MS detection results showed much higher concentration of ketamine and its metabolites present in mice urine, indicating that the urothelial toxicity may directly come from the high concentration of ketamine and its metabolites in mouse urine.

Body weight loss and voiding behavior dysfunction

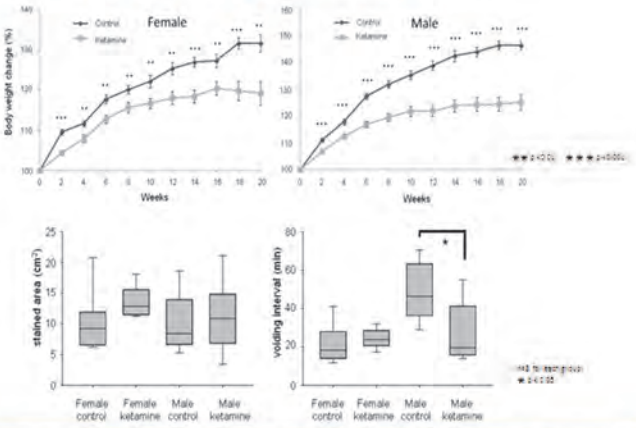

Body weight loss and urination dysfunction (especially in male mice) are likely associated with the chronic toxicity of long-term ketamine injection.

The potential DEGs of ketamine-treated mice (mixed with male & female mice)

Gene ID	Gene symbol	Official full name	Fold change	*P*-value
57256	Cxcl14	chemokine (C-X-C motif) ligand 14	0.787	9.49E-06
11687	Alox15	arachidonate 15-lipoxygenase	0.664	2.66E-03
59289	Ccbp2	chemokine binding protein 2	0.620	7.91E-05
12772	Ccr2	chemokine (C-C motif) receptor 2	0.999	1.05E-01#
20306	Ccl7	chemokine (C-C motif) ligand 7	0.820	1.04E-01#
12825	Col3a1	collagen, type III, alpha 1	0.676	2.35E-03
11839	Areg	amphiregulin	0.664	1.42E-02
12843	Col1a2	collagen, type I, alpha 2	0.654	4.06E-04
68568	Cthrc1	collagen triple helix repeat containing 1	0.609	2.25E-02
13614	Edn1	endothelin 1	0.695	1.04E-02
11504	Adamts1	a disintegrin-like and metallopeptidase with thrombospondin type 1 motif, 1	0.548	5.84E-03
12832	Col5a2	collagen, type V, alpha 2	0.521	2.43E-02
18613	Pecam1	platelet/endothelial cell adhesion molecule 1	0.517	1.10E-02

(# indicates the result does to significant)

- **Extracellular matrix related:** Col3a1, Col1a2, Col5a2, Cthrc1, Adamts1
- **Chemokine related:** Cxcl14, Ccbp2, Ccr2, Ccl7
- **Growth factor-like:** Areg, Edn1
- **Others:** Alox15, Pecam1 (CD31)

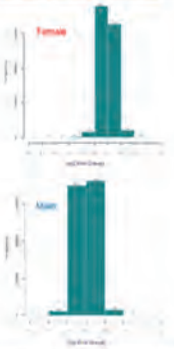

	up-regulated	down-regulated
Male	124	115
Female	156	190

The qRT-PCR verification and angiogenesis revealed by H&E stain

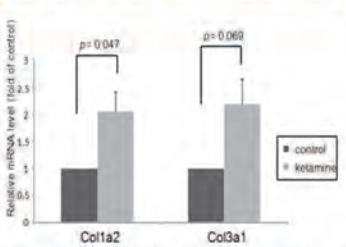

The mRNA samples are extracted from four control and three ketamine-treated group mice (normalized to the Actb mRNA. Data are presented as the mean ± SE)

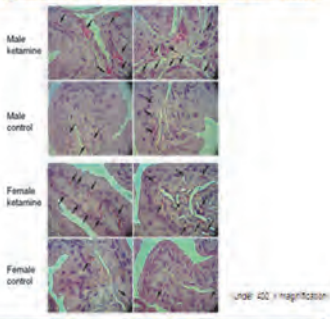

It revealed a number of gene expression involved in chronic wound healing response and collagen accumulation, which were closely related to fibrosis progression in the connective tissue.

Conclusions

- We claimed this is the first KIC animal experiment done on BALB/c mouse.
- Based on the evidence in our KIC mouse experiment, we may build up a mechanism that delineates fibrosis formation of urinary bladder induced by the pathogenesis of ketamine abuse.

Synthesis, cellular uptake and photocytotoxicity of 9-/13-lipophilic berberine derivatives as potential anticancer agents

Hong-Jhih Lin (林鴻志), Li-Chen Tsai (蔡立宸), Jou-Man Huang (黃柔嫚), Jin-Yi Wu (吳進益)*

Department of Microbiology, Immunology and Biopharmaceuticals, National Chiayi University, Chiayi, Taiwan

INTRODUCTION

Berberine is a quaternary ammonium salt from the protoberberine group of isoquinoline alkaloids. It has a wide range of biochemical and pharmacological effects. This study aims to synthesize lipophilic 9-/13-substituted berberine derivatives and evaluate the phototoxic activity against human cancer cell lines using MTT assay in vitro. In this report, our results revealed that the longer lipophilic substituents can increase both the cell uptake and the inhibition of cell growth on human cancer cell lines. These results suggested that the presence of lipophilic substituents with moderate sizes might be crucial for the optimal anticancer activity. In conclusion, it is confirmed berberine derivatives at 9-/13-position bearing long chain n-alkyl group as anti-cancer agents and also as potential adjuvant of phototoxic or chemotherapeutic drugs. The present work can be the evidence that berberine derivatives have potent anti-cancer activities against human liver cancer cells.

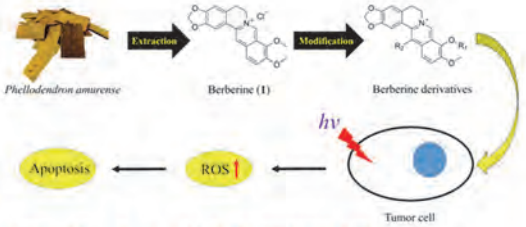

MATERIALS AND METHODS

Scheme 1: Synthesis of 9-/13-substituted berberine derivatives.

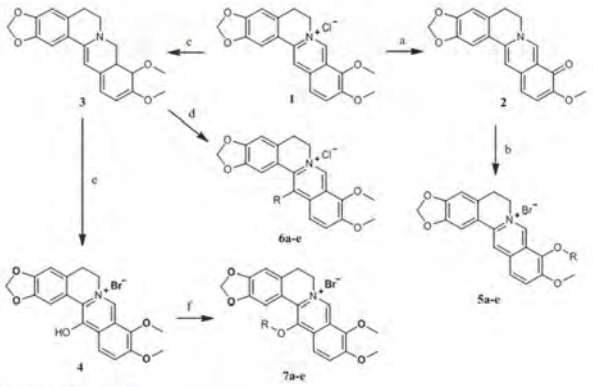

RESULTS

Table 1. IC_{50} values and lipophilicity of berberine and its derivatives on the growth of human cancer cell lines for 24 h

Compd	R	clog *P*	IC_{50} (μM) HepG2 Liver	BFTC905 Bladder	HT29 Colon
1	9-*O*-methyl	−0.38	> 40	26.11 ± 6.07	> 40
5a	9-*O*-butyl	1.20	8.27 ± 1.69	6.40 ± 2.20	> 15
5b	9-*O*-hexyl	2.26	2.83 ± 0.84	1.74 ± 0.22	14.70 ± 4.41
5c	9-*O*-octyl	3.32	0.59 ± 0.21	1.18 ± 0.31	3.88 ± 1.06
5d	9-*O*-decyl	4.37	0.61 ± 0.18	0.89 ± 0.11	2.79 ± 0.44
5e	9-*O*-dodecyl	6.49	0.32 ± 0.08	0.76 ± 0.02	1.34 ± 0.32
6a	13-butyl	1.31	8.11 ± 0.15	> 15	> 15
6b	13-hexyl	2.37	2.19 ± 0.42	9.76 ± 1.02	8.45 ± 0.16
6c	13-octyl	3.81	1.19 ± 0.32	1.08 ± 0.23	2.77 ± 0.03
6d	13-decyl	4.87	0.67 ± 0.19	0.75 ± 0.19	1.76 ± 0.64
6e	13-dodecyl	5.54	0.77 ± 0.18	0.87 ± 0.15	1.39 ± 0.08
7a	13-*O*-butyl	1.37	8.21 ± 1.47	9.94 ± 1.70	> 20
7b	13-*O*-hexyl	2.43	2.64 ± 0.31	2.09 ± 0.47	5.69 ± 0.66
7c	13-*O*-octyl	3.49	0.98 ± 0.26	1.00 ± 0.24	2.21 ± 0.21
7d	13-*O*-decyl	4.54	0.91 ± 0.40	0.96 ± 0.29	1.39 ± 0.19
7e	13-*O*-dodecyl	5.60	0.83 ± 0.30	0.78 ± 0.13	1.23 ± 0.06

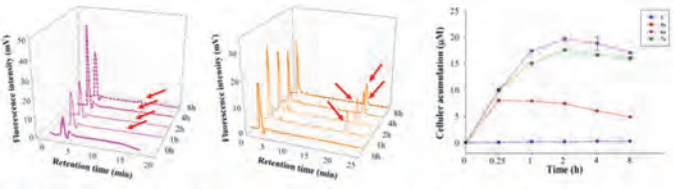

Figure 1. HPLC analysis of compounds **1** (10 μM) (left), **7e** (10 μM) (middle) in HepG2 for 0–8 h; (right) Cellular accumulation of compounds **1**, **5e**, **6e** and **7e** in HepG2 after treatment 10 μM for 0–8 h.

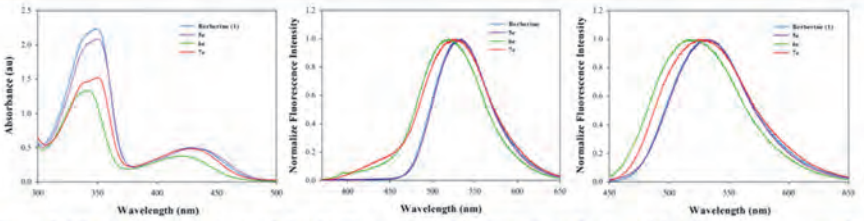

Figure 2. UV-vis absorption spectra (left) of berberine (**1**) and its derivatives (**5e**, **6e** and **7e**), fluorescence spectra by excitation at 352 nm (middle) and 420 nm (right).

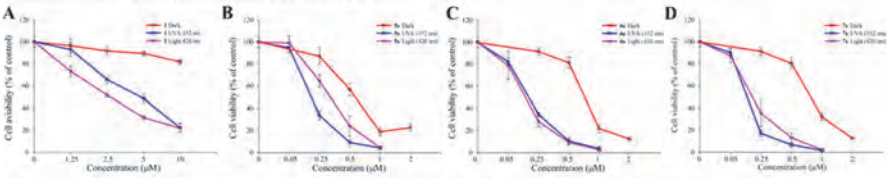

Figure 3. Cell viability of berberine and its derivatives on HepG2 in the dark and after PDT for 24 h.

Table 2. IC_{50} values of berberine and its derivatives on HepG2 in the dark and after PDT for 24 h.

Cell line	Compd	IC_{50} (μM) Dark	UVA (352 nm)	PIF (Dark/UVA)	Light (420 nm)	PIF (Dark/Light)
HepG2	**1**	> 40	3.92 ± 1.04	> 10.2	3.48 ± 0.69	> 11.5
	5e	0.52 ± 0.17	0.41 ± 0.28	1.2	0.28 ± 0.15	1.9
	6e	1.42 ± 0.38	0.15 ± 0.01	9.5	0.15 ± 0.06	9.5
	7e	1.66 ± 0.48	0.15 ± 0.03	11.1	0.14 ± 0.06	11.9
HT29	**1**	>40	35.28 ± 1.38	> 1.1	>40	> 1
	5e	3.42 ± 0.79	0.39 ± 0.03	8.7	0.78 ± 0.25	4.3
	6e	3.04 ± 0.32	0.23 ± 0.05	13.2	0.28 ± 0.02	10.8
	7e	2.64 ± 0.44	0.19 ± 0.07	13.8	0.23 ± 0.02	11.4
BFTC905	**1**	>40	14.12 ± 1.94	> 2.8	15.20 ± 1.74	> 2.6
	5e	2.74 ± 0.66	0.22 ± 0.08	12.4	0.29 ± 0.11	9.4
	6e	2.58 ± 0.87	0.18 ± 0.06	14.3	0.20 ± 0.09	12.9
	7e	2.64 ± 0.33	0.14 ± 0.04	18.8	0.17 ± 0.05	15.5

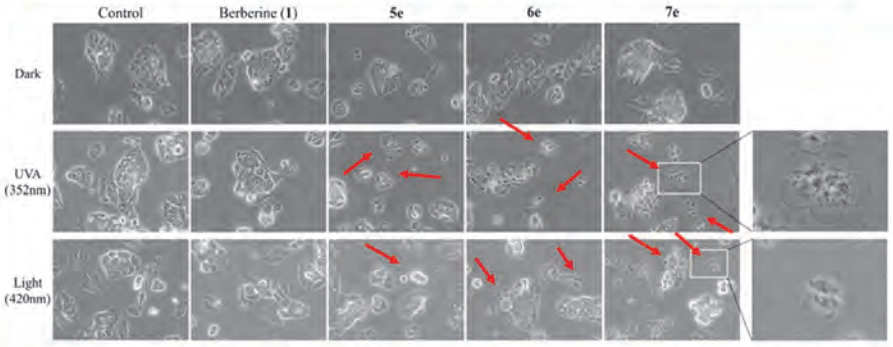

Figure 4. Cell morphological change of HepG2 cell lines exposure without (control) or with 0.5 μM **1**, **5e**, **6e** and **7e** in the dark or light (352 nm or 420 nm) after 24 h.

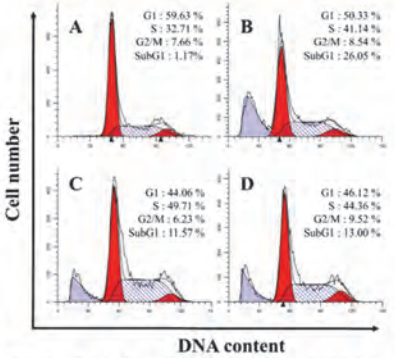

Figure 5. Cell cycle distribution changed by treatment with **1** (A), **5e** (B), **6e** (C), **7e** (D) at 0.5 μM concentration on HepG2 for 24 h with irradiation (5.6 mW/cm², 10 min).

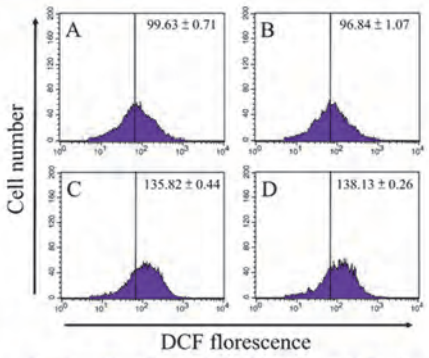

Figure 6. The effects of HepG2 treated with **7e** (0.1 μM) after radiation on percentage distribution of ROS by DCFH-DA staining. (A) Dark, (B) Dark and treated with **7e** for 4 h, (C) and (D) Light (420 nm, 10 min) treated with **7e** for 2 h and 4 h.

CONCLUSIONS

The introduction of long chain *n*-alkyl groups at the 9-/13-position of berberine was to evaluated anti-cancer activity and the cellular uptake was to analyze by HPLC test. The photocytotoxicity test confirmed that compounds **1**, **6e** and **7e** increased the cytotoxicity after radiation. Cell membrane blebbing showed that the image and cell cycle proved compounds **6e** and **7e** induced cell apoptosis. We found that the compound **7e** increased the content of ROS in the HepG2 cells after irradiation. In present study, the berberine derivatives to be developed as newly photocytotoxic anti-cancer agents.

Investigate of the association between biofilm formation activity and microsatellite typing in *Candida albicans* clinical isolates

Jia-Yuan Chang (張家源)[1], 盧章智 (Jang-Jih Lu)[2] and Shao-Hung Wang (王紹鴻)[1]
[1]Departmant of Microbiology, Immunology and Biopharmaceutical, National Chiayi University
[2]Department of Laboratory Medicine, Chang-Gung Memorial Hospital Linkou

Abstract

Introduction: *Candida albicans* is one of the most frequent causes of hospital-acquired infections. Biofilm formed on artificial surface, such as invasive medical equipment or catheter device, strongly increases resistance against anti-fungals. Moreover, the persistent infection leads to uncontrolled severe systemic infection. Microsatellite, a polymorphic sequence repeats of two to six base-pair in length, is widely used in the analyses of genetic relationship and diversity. Recent studies showed microsatellite CAI genotype distribution of *C. albicans* strains correlates with the severity of vulvovaginal candidiasis. In previous studies, 325 *Candida albicans* isolates collected from Chang Gung Memorial Hospital at Linkou (CGMHL) during 2003-2011 were molecular typed by MLST. DST659 genotype, a major genotypes in CGMHL isolates, formed stronger biofilm than other DST genotypes. Aim: The current study is aimed to investigate the association between biofilm formation activity and microsatellite genotyping in *C. albicans* clinical isolates. Materials and methods: 325 *C. albicans* isolates collected from CGMHL, 2003 to 2011, were MLST typed with seven selected house-keeping gene loci. Biofilm formation ability of dominant DST isolates were analyzed in vitro by a filter weighting assay. Zebrafish egg infection assay was used to detect the biofilm effects in vivo. Five sets of microsatellite, CAI, CAIII, CAV~CAVII, were used to genotype *Candida* isolates. Results: Two major MLST genotypes DST693 and DST659 were found in 325 CGMHL isolates. Biofilm formation in DST659 isolates is higher than DST693 by both in vitro and in vivo assays. DST659 group can be divided into three CAI genotypes, including types 11-20, 11-21 and 11-11. CAI genotype 11-11 may represent as a low biofilm marker.

Results

UPGMA分析林口長庚醫院 *C. albicans*臨床菌株之分子譜系

325株菌株經MLST分析與全球資料庫比對，再以UPGMA分析譜系，結果如Figure 1。兩大基因型中，DST659位於全球第四分群(clade 4)、DST693 群列為亞洲所特有第十九分群(clade 19)。

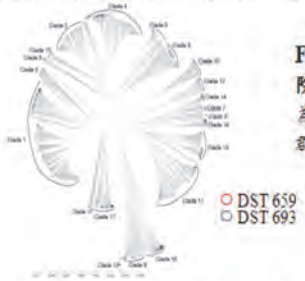

Figure 1. UPGMA分析林口長庚醫院*C. albicans*菌株譜系。 紅色表示為DST659群，藍色表示為DST693群，綠色表示為DST669群。

主要基因型菌株生物膜形成能力分析

DST659、DST693、DST669 菌株以秤重分析其生物膜形成能力，結果顯示其中以DST659 群生物膜形成能力較強，如 Figure 2。斑馬魚卵感染試驗分析結果顯示，DST659感染魚卵存活率較DST693低，如 Figure 3。此外，體外生物膜分析發現DST659 群菌株可再分為生物膜強、弱兩群，如 Figure 4。

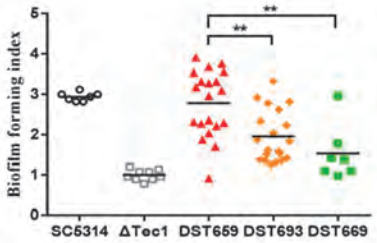

Figure 2. 體外生物膜秤重分析DST659、DST693、DST669。 *C. albicans* SC5314 作為陽性對照組；*ΔTec1*為*Tec1*基因突變株作為陰性對照組。**表示與DST659 相比具有顯著差異，$P<0.01$。

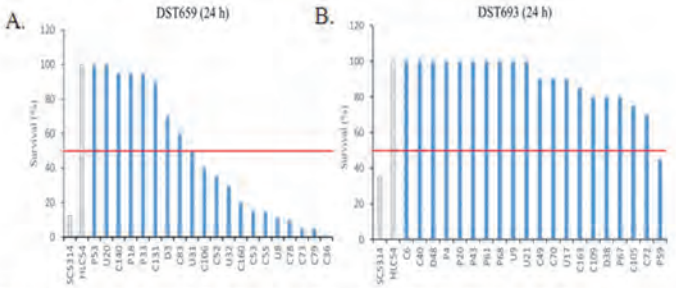

Figure 3. 斑馬魚卵感染試驗分析DST659、DST693生物膜毒性。 *C. albicans* SC5314 作為陽性對照組；HLC54 為*CPH1*及*EFG1*基因突變株，作為陰性對照組。 (A) DST659菌株感染魚卵24小時後之存活率，(B) DST693菌株感染魚卵24小時後之存活率。

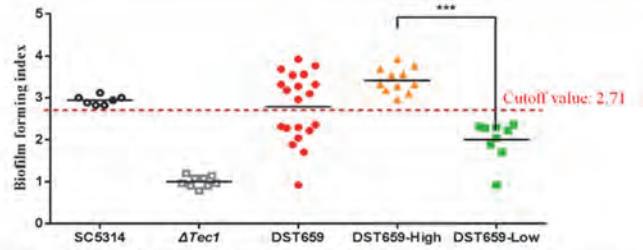

Figure 4. 體外生物膜秤重分析DST659-High、DST659-Low。 *C. albicans* SC5314 為陽性對照組；*ΔTec1*為*Tec1* 基因突變株，作為陰性對照。DST659-High與DST659-Low是利用K-means clustering分群(SPSS)。***表示與 DST659-High 相比具顯著性差異，$P<0.001$。

Microsatellite PCR分析 DST659-High 與 DST659-Low 菌株之基因分型

以 CAI 引子對DST659-High 與 DST659-Low 兩臨床菌進行PCR 增幅進行分型，結果如 Figure 5。Microsatellite CAI基因分型分析DST659群結果如 Table 1.所示，可分成三種基因型11-20、11-21、11-11，其中基因型11-11菌株皆為生物膜能形成能力弱的菌株。

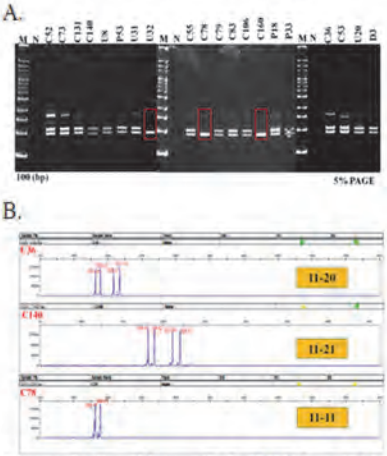

Table 1. CAI基因分型分析DST659群生物膜形成能力。

Genotype observed	Biofilm formation ability	*C. albicans* isolates	Total number
11-20	High	C036, C052, C053, C073, C131, D08	6
11-20	Low	C055, C079, C83, C106, D003, P018, P033, P053, U020, U031	10
11-21	High	C140	1
11-11	Low	C079, C160, U032	3
			20

Figure 5. *C. albicans* 染色體DNA以 CAI 微衛星引子增幅之膠體電泳結果 (A)，以及GeneScan 分析結果(B)。

Conclusion

- DST659 群生物膜形成能力較DST693 及 DST669 強。
- DST659 群可區分為生物膜形成能力強、弱兩群。
- CAI 基因型 11-11 可能做為弱生物膜的基因標記。